Fragility Curves for Vulnerability Assessment of Steel Moment-Resisting Frames Adjacent to Slopes

Jafar Mohammadi[1], Gholam Reza Nouri[2*], Ali Ghanbari[3], and Amid Erfani[1]

1. M.Sc. Graduate, Kharazmi University, Tehran, Iran
2. Assistant Professor, Kharazmi University, Tehran, Iran, *Corresponding Author; email: r.nouri@khu.ac.ir
3. Professor, Kharazmi University, Tehran, Iran

Received: 01/03/2016
Accepted: 28/02/2017

ABSTRACT

Observations from past earthquakes in addition to the results from analytical and numerical studies have shown that topographic irregularities significantly affect seismic site responses. Nonetheless, few studies have focused on the effect of topography amplification on the seismic vulnerability of buildings adjacent to slopes. In this study, using "match up damage index to damage thresholds" method introduced in HAZUS, fragility curves were developed for steel moment-resisting frames (SMRF) built adjacent to slopes. A two-dimensional finite-element model of the soil was implemented in ABAQUS to develop the fragility curves. Six models of combination of soil-structure and topography were considered. Furthermore, three types of buildings at different distances from the crest of the slope were considered. The results indicated that slope effect leads to up to 37% increase in the damage probability and illustrated that amplification factor had a range of 1.1 to 1.35, moreover, in comparison with slight states, the probability damage growth rate in moderate and extensive states are higher.

Keywords:
Fragility curve;
Topography;
Vulnerability;
Earthquake

1. Introduction

According to HAZUS, the fragility curves of the buildings are obtained using the median values of interstory drift ratio of the building, defined in four damage states of low, medium, extensive and complete. Generally, the damage is estimated based on several parameters such as type of the building, height of the building, and level of seismic design. A complete list of the limit states used to create the fragility curves for various types of buildings is available in HAZUS [1]. Based on another classification, the fragility curves are sub-divided into empirical, expert judgment, analytical, and hybrid fragility curves. The empirical curves are obtained by investigating the performance of the buildings in the past earthquakes and previous observations. However, with the development of computational tools and new techniques, the analytical methods were created. These methods may contain a nonlinear analysis of the buildings, probabilistic modeling of earthquakes and generalization of the results of a small area to a large area. In the hybrid method, the fragility curves are obtained by combining different methods [2]. Researchers such as, Singhal and Kiremidjian [3], Rossetto and Elnashai [4], Ellinwood [5], developed different analytical fragility curves for structures. Furthermore, in Hazus (1999) the fragility curves are presented for

36 types of buildings, based on the type of structural system, height and design level. Moreover, Saez et al [6] presented fragility curves for steel moment-resisting frames considering soil-structure interactions.

As mentioned above, although fragility curves for different types of buildings have been represented in different studies, the effect of some contributing factors such as soil-structure interaction and topography amplification on the building seismic vulnerability are not well understood and quantified. On the other hand, many parameters such as properties of the subsurface layer materials, topography, properties of the input motion can have an effect on the soil-structure interaction and the building vulnerability [7].

To investigate the topography effects, various assumptions such as considering the rigid and compliant bedrock, half space, stimulations with different frequencies, slopes with different angles, different heights of slopes, and soil type were evaluated [7]. Topographic amplification factors at the crest of the slope, derived by Ashford et al (1997) as illustrated for different values of the slope angle in Figure (1). Generally, it can be concluded that topography induced amplification value increases with increasing of the slope angle [8-9].

Topography effect was investigated using field and numerical methods. Different methods such as the finite-element, boundary element, discrete element, spectral element method or a combination of the mentioned methods has been used for numerical assessment of the effects of topography. Some of these studies achieved the range of 2 to 3 times for amplification factor [10].

Using finite element method, Rizzitano et al [7] assessed the effect of slope inclination, frequency content of motion by considering three cases of homogeneous half-space soil, slopes overlying either rigid or compliant bedrock. They concluded that there is a complicated interaction between soil behavior and effects of the topography on the amplification of shallow ground movement which cannot be evaluated separately. They also stated that non-linear behavior of soil would provide more acceptable results [7]. Assimaki and Kausel [11] presented pattern variation of amplification of motions due to the presence of structure adjacent to the slope. The elastic parametric investigation illustrated clearly that the presence of a structure affecting the time- and frequency-domain characteristics of response, not only at the location of the structure, but also along the surface behind the crest and along slope toward the cliff toe. Topographic amplification, however, was primarily restricted in the vicinity of the foundation, and strongly decreased thereafter. Nonetheless, the overall site and topography effects behind the crest were practically the same as in the free field. It was clarified that, the peak vertical acceleration was shown to be on the same order of magnitude for all the analyzed cases.

In this paper, by developing fragility curves, effects of topography amplification on the damage probability of the buildings adjacent to slopes will be investigated.

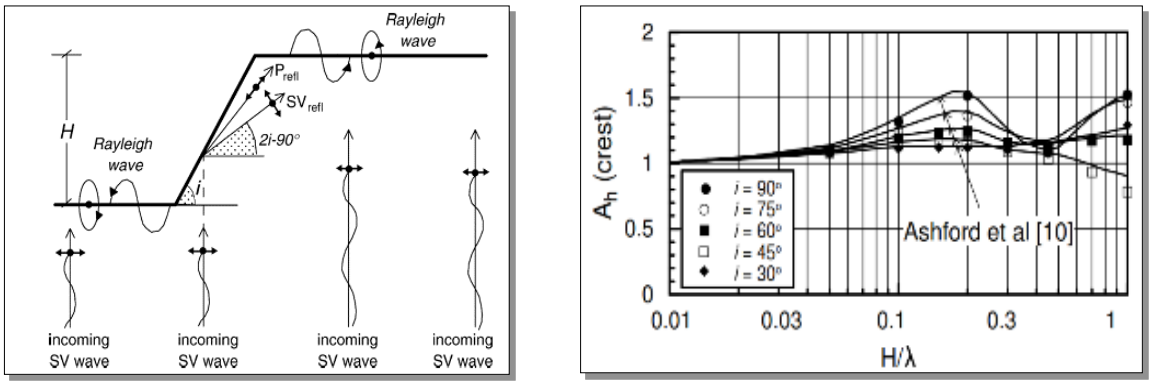

Figure 1. Schematic illustration of incoming SV waves and induced P_{ref}, SV_{ref} and Rayleigh in the case of step-like slopes and topographic amplification factors [8-9]**.**

2. Methodology of Fragility Analysis

Building damages can be divided into several distinct damage states. The probability of exceedance from a damage state for strong ground motion intensity (IM) is calculated using Eq. (1) [12].

$$F_i\,(im) = P(D > d_i \mid IM = im) \tag{1}$$

where, $F_i\,(im)$ is the probability of exceeding damage D from damage stated at given ground motion $IM=im$. The cumulative distribution function for each im is obtained by Eq. (2) [12].

$$\begin{aligned} &F_i\,(im)=P(D> di \mid IM=im)= \\ &1- F_{im}\,(d_{it}) =1-\int_{-\infty}^{d_{it}} f_{im}(d_i)d(d_i) \end{aligned} \tag{2}$$

The exceeding probability from each damage level can be calculated using Eq. (3) [13].

$$\begin{aligned} F_i\,(pga) &= P(D > d_i \mid PGA = pga) \\ &= 1 - P(D \le d_i \mid PGA = pga) \\ &= 1 - \varphi\left(\frac{1}{\beta_{sd}}.Ln\left(\frac{ISD_i}{\overline{ISD}}\right)\right) \end{aligned} \tag{3}$$

where, assuming the parameter *PGA* as *IM*, the probability of exceedance of the maximum interstory drift of the stories (*ISD*) is calculated from the limits introduced in HAZUS. Ø is the normal distribution function, β_{sd} is standard deviation data, ISD_i is the introduced relative drift as the damage threshold in each damage state, and *ISD* is the mean of the frame interstory drifts in each analysis. Finally, the fragility function is obtained using Eq. (4) and proper fitting of the function to the fragility points [12].

$$\begin{aligned} F_i\,(pga) &= P(D > d_i \mid PGA = pga) \\ &= \varphi\left(\frac{1}{\beta_{sd}}.Ln\left(\frac{pga_i}{\overline{PGA}}\right)\right) \end{aligned} \tag{4}$$

3. Properties of Structure, Slope and Soil Modeling

In this paper, three steel moment resistant frame (SMRF) which have been designed [13] based on EC3 [14] and EC8 [15] were examined. These structures have 3 bays, and 6, 9, 12 stories. The length of each bay and the height of each story are 5 and 3 m, respectively. The frames were modeled as 2D in ABAQUS software. A36 steel material is used in the models and the yield strength of steel is 235 MPa. Von-Mises yield criterion was applied to the non-linear behavior of materials. A kinematic material hardening of 3% is assumed for the nonlinear elements and damping is the Rayleigh-type damping. Rayleigh damping is viscous damping that is proportional to a linear combination of mass and stiffness. The damping matrix C is given by Eq. (5). According to Zerwer et al [16], the coefficients α and β corresponding to the stiffness matrix is obtained via Eqs. (6) and (7).

$$[C] = \alpha[M] + \beta[K] \tag{5}$$

$$\alpha = \xi\left(\frac{2\omega_1\omega_2}{\omega_1 + \omega_2}\right) \tag{6}$$

$$\beta = \xi\left(\frac{2}{\omega_1 + \omega_2}\right) \tag{7}$$

where, *[C]* is damping matrix, *[M]* is mass matrix and *[K]* is stiffness matrixes. ω_1 and ω_2 are respectively the first and second natural angular frequencies obtaining from the frequency analysis.

Table (1) shows properties of the frames and fundamental period of the examined structures both with soil structure interaction (T_{SSI}) and without SSI (T_{FIX}).

Table 1. Section frame and fundamental period of frame [13].

No.	Number of Building Story	Columns HEB (Number of Story) – Beams IPE (Number of Story)	T_{fix}(s)	T_{ssi} (s)
1	6	280-360(1-4)+ 260-330(5-6)	1.12	1.319
2	9	340-360(1)+340-400(2-5)+320-360(6-7)+300-330(8-9)	1.45	1.683
3	12	400-360(1)+400-400(2-3)+400-450(4-5)+360-400(6-7)+340-400(8-9)+340-360(10)+340-330(11-12)	1.706	2.097

The desired slope has a height of 30 m with the soil properties as illustrated in Table (2) [18]. The depth of the bedrock is considered equal to 60 m. A schematic illustration of the 2D analyzed mesh and the boundary condition is provided in Figures (2) and (3).

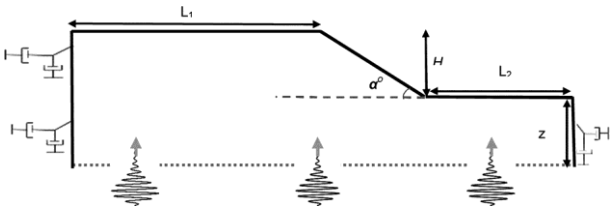

Figure 2. Schematic illustration of finite difference model for the numerical analyses of slope topography effects.

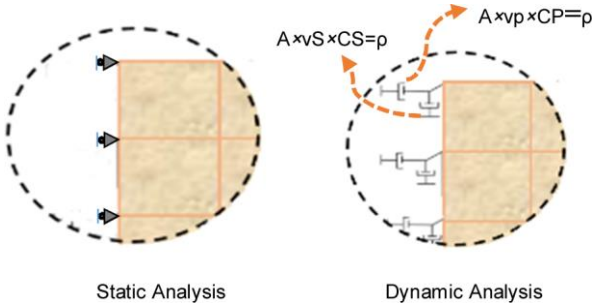

Figure 3. Boundary conditions in static and dynamic steps.

The Mohr-Coulomb criterion is used for soil; parameters for this model are described in Table (2). This model is based on the plane strain conditions, and shear criterion is characterized by friction angle and cohesion represented. Rayleigh method was used for modeling the soil damping, so that, ω_1 was taken as the first natural frequency of the 1D system corresponding to a soil column behind the slope crest and ω_2 was the predominant frequency of the input motions [10].

Table 2. Soil properties [17].

ρ (kg/m3)	1800
C, (Kpa)	70
Ø	31
ν	0.35
Vs(m/s)	238

Besides, to reduce the effects of the boundaries, the horizontal distance of the boundary from the slope is considered sufficiently large (L1= L2 = 400m). Six different combinations of soil-structure and topography are considered for models (Figures 4 and 5).

Eight-node tetrahedron elements are used. According to Rizzitano et al [7], to avoid filtering the high-frequency components of the input seismic motions during the propagation process and to ensure the accuracy of the numerical solution, the height (h) and the width (L) of the elements of the mesh were selected according to Eq. (8).

$$h \le (1/8 - 1/5)Vs / f_{\max} \quad \text{and} \quad l \le 5h \tag{8}$$

where V_s and f_{max} are the soil shear-wave velocity in the element and maximum frequency of the considered input motion, respectively.

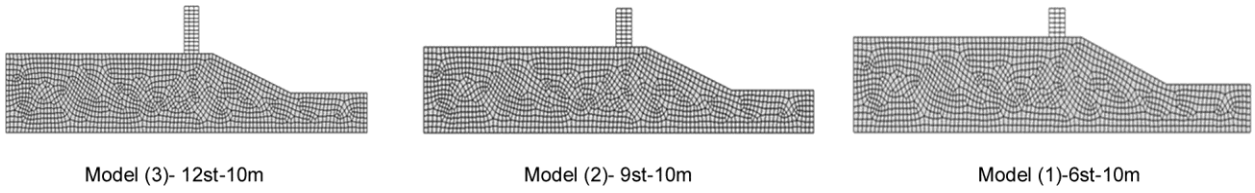

Figure 4. Schematic illustration of soil-structure-topography models.

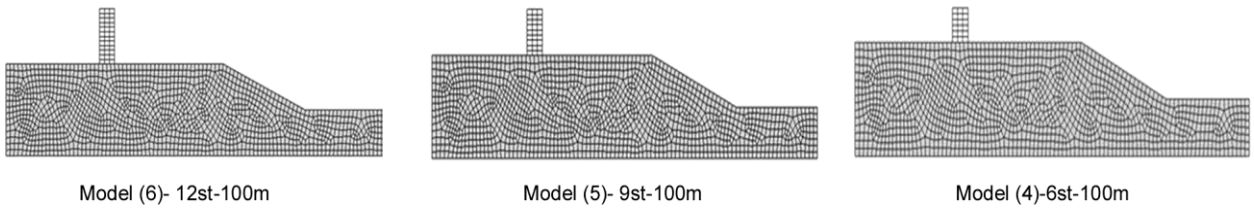

Figure 5. Schematic illustration of soil-structure-topography models.

4. Verification of Modeling

In order to investigate the accuracy of the soil modeling, a slope with α= 90° is modeled [9]. The slope height H = 50 m and the thickness of the soil deposit *D* = 200 m were assumed in order to compare the results of Tripe et al [10].

The fundamental frequency of the considered soil deposit behind the crest of the slope, evaluated according to 1D shear wave propagation theory, is f1=Vs/4(H+D)=0.5 Hz. The input motions have amplitude a_o=0.1g and frequencies (f) equal to 0.1, 0.5, 1, 1.5, 2, 3, 5 and 10 Hz; accordingly, eight values of the normalized frequency f in the range of 0.01–1 were considered. The results of the analyses are plotted in terms of horizontal peak acceleration at free-field boundaries $a_{h,ff}$ and at the crest of the slope $a_{h,max}$. A sinusoidal harmonic motion with amplitude of 0.1g was used. Figure (6) shows that the results are in good agreement.

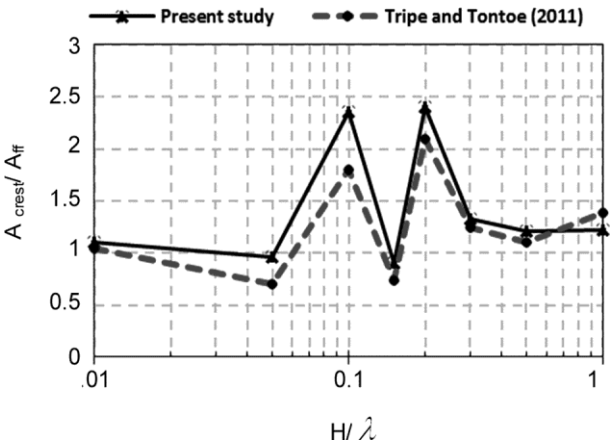

Figure 6. Topographic amplification factors: current study versus Tripe et al [10].

5. Ground Motion

Since this study investigates the effects of different input ground motion on the seismic vulnerability of the buildings adjacent to slope, an appropriate number of records should be considered. Bazazura and Cornell [18] proposed 10 to 20 records for assessment of the fragility analysis. In this study, to estimate the distribution of response, 10 records on the bedrock (shear wave velocity is more than 650 m/s) have been used. To reduce the near source effect, records are selected in such a way that they have no pulse in velocity time history and distance from source to site greater than 10 km considered [19-20]. The comparison between the design code spectrum [21] and the elastic spectra of the selected ground motion records is given in Figure (7). The characteristics of the selected ground motion records are listed in Table (3).

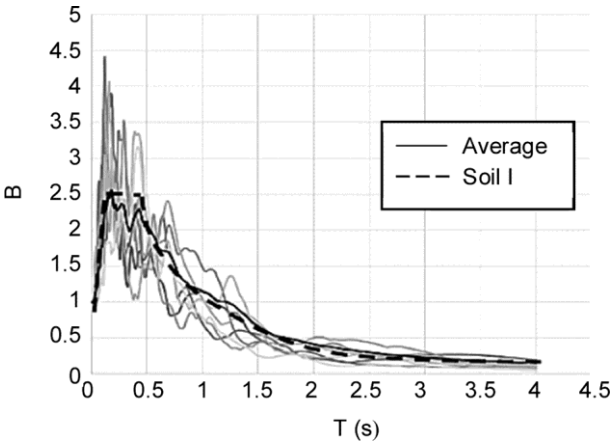

Figure 7. Normalized elastic response spectrums of the input records and Iranian code-2800 [21].

Table 3. Selected records for fragility analysis.

	Event	Station	M	Vs (m/s)	R (KM)
1	San Fernando	Cedar Springs	6.61	813.48	89
2	Loma Prieta	San Jose-Santa	6.93	681	14.7
3	Hector	Hector	7.13	726	11.6
4	Northridge-01	Lake Hughes#4	6.69	600	31.6
5	Loma Prieta	SF-Cliff House	6.93	614	78
6	Iwate	Minase Yuzawa	6.9	655	21
7	Umbria Marche	Norcia	5.6	678	19
8	Taiwan SMART	SMART1(45)	7.3	671	51.35
9	Chi-Chi	Tcu138	6.2	652.8	22.14
10	Chuetsu-Oki	Joetsu Yanagishima	6.8	605	31

6. Fragility Curves

The fragility curves presented in this section are developed through a series of nonlinear time history analyses at different intensities of earthquake excitation. Six models of soil-structure and slope are used. As indicated in Figures (2) and (3), 6-, 9- and 12-story frames located at 10 m and 100 m from the crest. Note that the response at the distance of 100 m was considered as a free-field response.

To prevent the sliding of slopes in the high levels of acceleration and also to prevent the effects of the slope displacement on the results pertaining to the effects of wave's reflection, the PGA values are limited to 0.5g, and the fragility curves are drawn in three damage states of low, medium and extensive. It should be noted that fragility curves were obtained based on bedrock motions. Tables (4) and (5) indicate the values of horizontal acceleration on the soil surface for both near and far distance from the slope. It can be derived that topography amplification (A_{crest}/A_{ff}) ranges from 1.1 to 1.35. Moreover, Figures (8) and (9) indicate the horizontal acceleration time history of two events on the bedrock and surface (10 m and 100 m).

To obtain the exceeding probability value of interstory drift derived from the analyses, the results were compared with limit states presented in HAZUS, in accordance with Table (6).

Table 4. Horizontal acceleration on bedrock and soil surface -100m.

$PGA_{surface}$	PGA_{base}
0.1g~0.125g	0.05g
0.2g~0.25g	0.1g
0.3g~0.375g	0.15g
0.4g~0.5g	0.2g
0.5g~0.625g	0.25g
0.6g~0.75g	0.3g
0.7g~0.875g	0.35g
0.8g~1g	0.4g
0.9g~1.125g	0.45g
1g~1.25g	0.5g

Table 5. Horizontal acceleration on bedrock and soil surface -10m.

$PGA_{surface}$	PGA_{base}
0.125g~0.15g	0.05g
0.25g~0.3g	0.1g
0.375g~0.45g	0.15g
0.5g~0.6g	0.2g
0.625g~0.75g	0.25g
0.75g~0.9g	0.3g
0.875g~1.05g	0.35g
1g~1.2g	0.4g
1.125g~1.35g	0.45g
1.25g~1.5g	0.5g

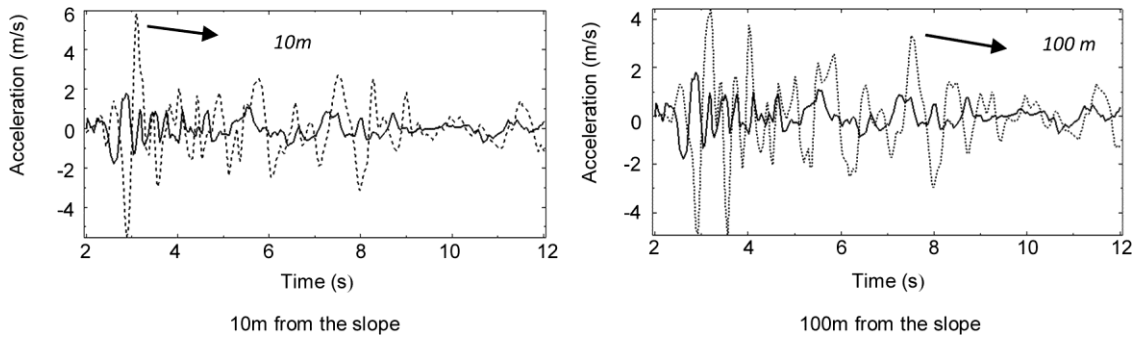

Figure 8. Horizontal acceleration on the soil surface (Event 1).

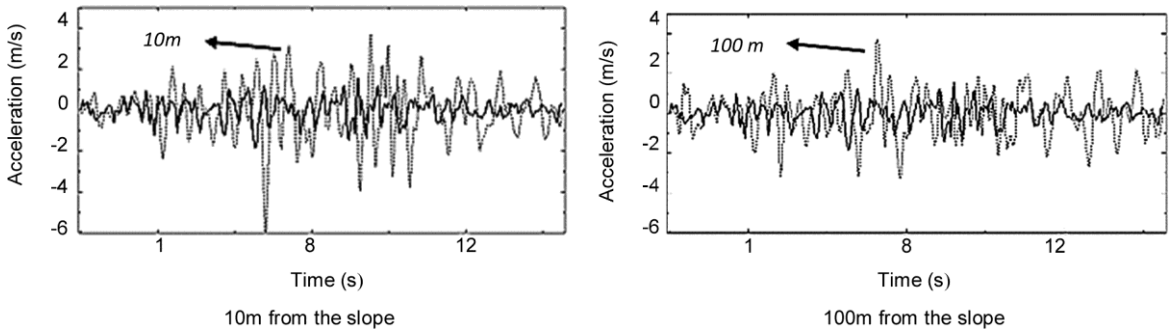

Figure 9. Horizontal acceleration on the soil surface (Event 8).

Table 6. Interstory drift at threshold of damage state (high code) [1].

	Slight	Moderate	Extensive	Complete
$SMRF_{(Mid\text{-}Rise)}$	0.004	0.008	0.02	0.0533
$SMRF_{(High\text{-}Rise)}$	0.003	0.006	0.015	0.04

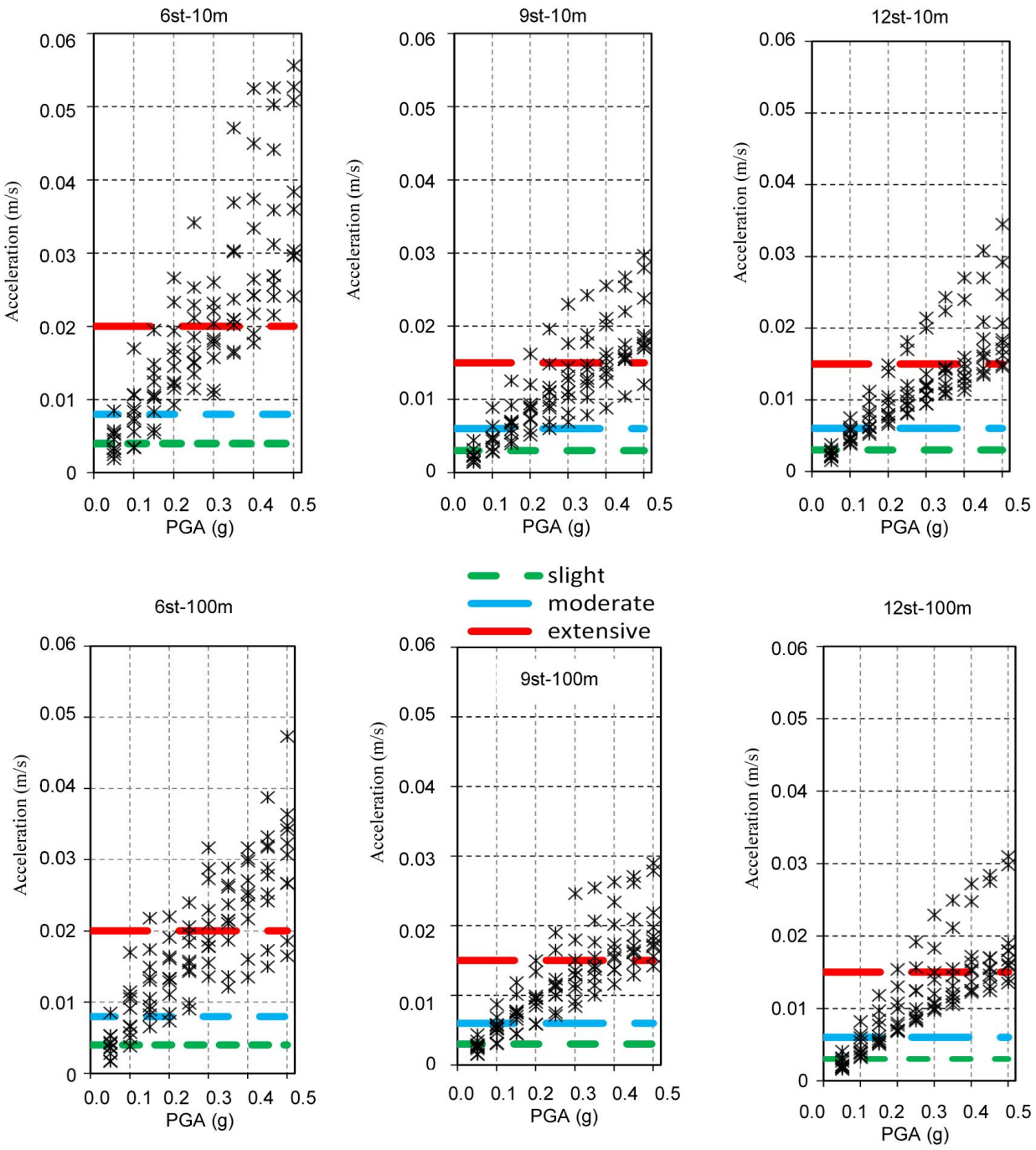

Figure 10. Distribution mode of the maximum interstory drift of stories of all the records in all scales.

Figure (10) shows the distribution of the maximum interstory drift in all scales. The mean damage threshold existing in HAZUS also are shown in Figure (10). Using Eq. (3) the fragility points were obtained for each model, and using a log-normal distribution and proper fitting, the fragility curves were obtained for all models in accordance with Figures (11) and (12-a), Table (7).

Fragility curves of the buildings located in the distance of 100 meters are representative of the fragility curves of frames in free field, therefore, the increase in vulnerability and damage probability is only due to the amplification of the slope. Figure (12-b), illustrates the probability damage growth rate of three frames in three damage states. According to results, the probability damage growth rate in moderate and extensive are higher than the slight states.

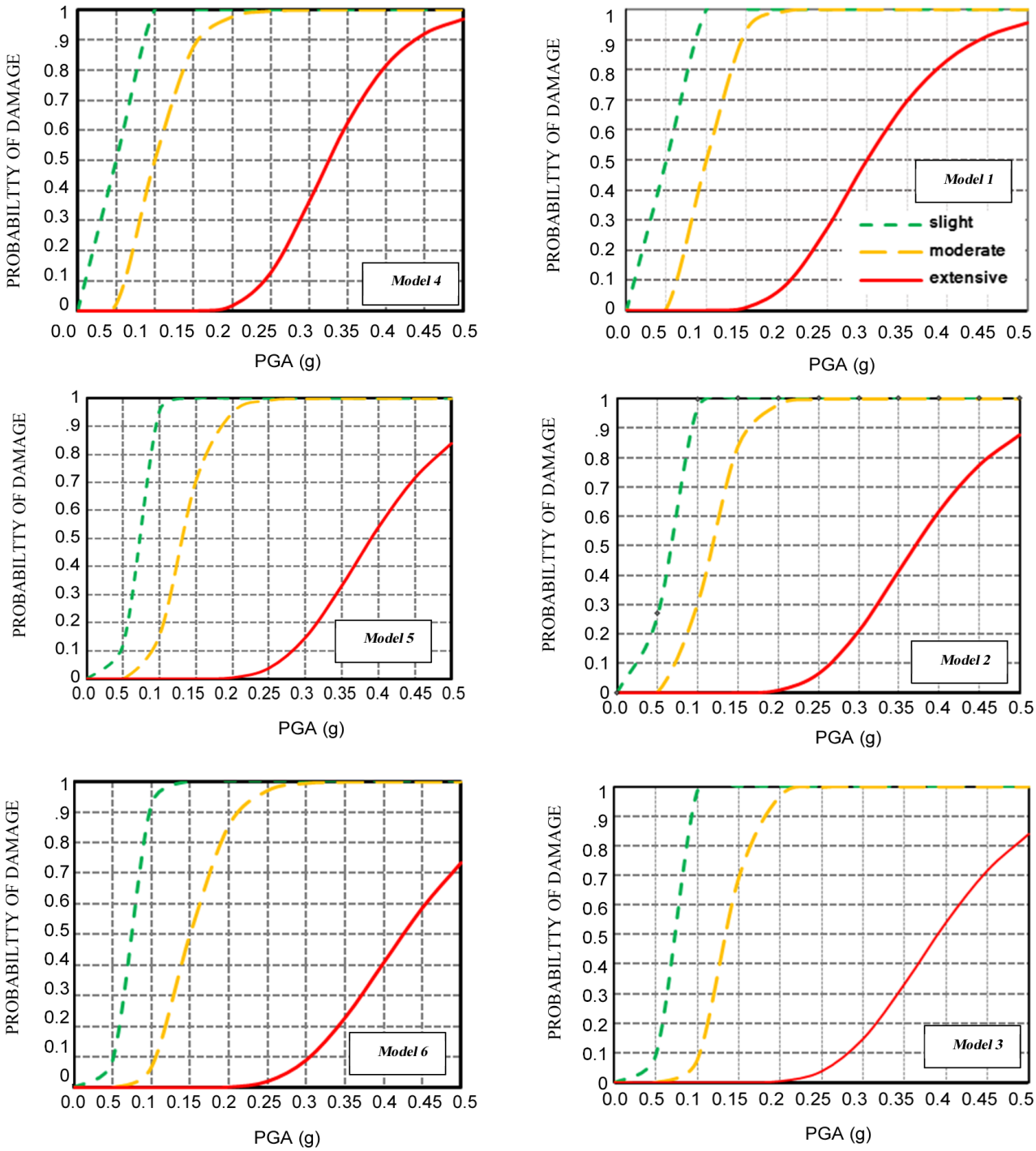

Figure 11. Fragility curves for buildings located 100m and 10m from the slope.

Table 7. Parameters of fragility curves.

	12st		9st		6st	
	100m	10m	100m	10m	100m	10m
	Deviation		Deviation		Deviation	
Slight	0.25	0.2	0.24	0.28	0.19	0.2
Moderate	0.27	0.21	0.26	0.27	0.35	0.27
Extensive	0.26	0.25	0.25	0.26	0.23	0.3
	Mean		Mean		Mean	
Slight	0.07g	0.065g	0.066g	0.06g	0.05g	0.05g
Moderate	0.15g	0.135g	0.13g	0.115g	0.1g	0.1g
Extensive	0.425g	0.39g	0.39	0.37g	0.325g	0.3g

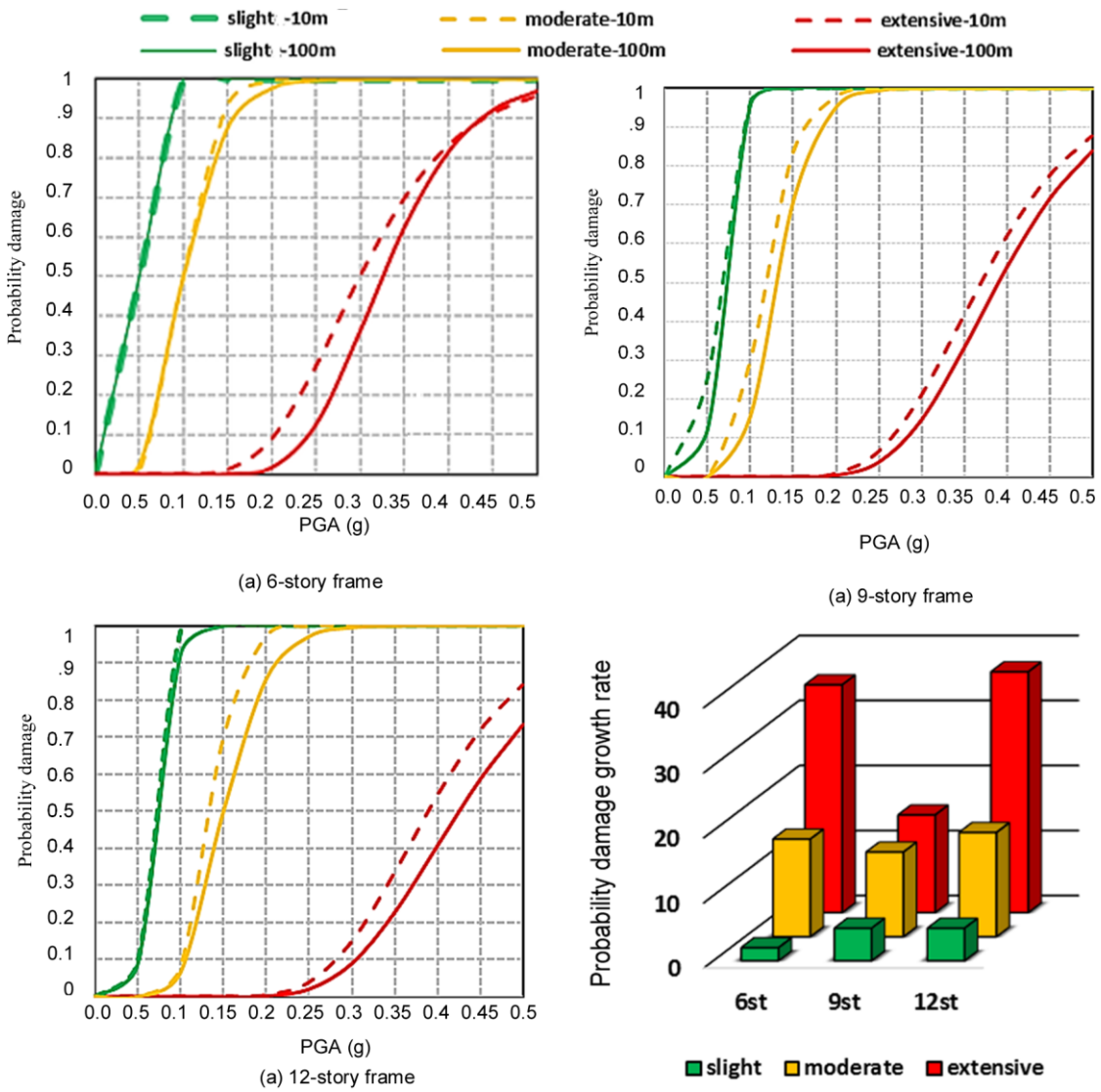

Figure 12. (a) Comparison of fragility curves (b) Probability damage growth rate of three frames.

Likely, this increase has its root in non-linear behaviors of both the structure and the soil.

According to fragility curves, topography amplification leads to an increase in slight, moderate and extensive damage in the range of 0-6%, 0-16% and 0-37%, respectively.

7. Conclusions

Topography effect on the assessment of the seismic vulnerability of SMRF was presented in this paper. The results illustrated that amplification factor had a range of 1.1 to 1.35; that is compatible with other studies.

The fragility curves were presented in three damage states. Comparing the fragility curves for the frames adjacent to slope (10 m far from crest) with those farther away (100 m far from crest) clearly showed an increase in the damage probability (0-37 %) with regards to the topography amplification.

However, in this study assessment of damage probability of frames were estimated based on mean of nonlinear response, different intensity range was monitored under different earthquake records.

Mode shapes of structures are considered and it showed topography affecting the structural properties. Subsequently, the mentioned reason maybe justifies the different pattern in response of the 9-story frame.

In comparison with slight states, the probability damage growth rate in moderate and extensive states are higher. Likely, this increase has its root

in non-linear behavior of structure and soil. Accordingly, the study of seismic vulnerability of building adjacent to slope is a considerable subject. Besides, it should be noted that current study has only examined a specific type of slope, and as a result, further studies are required to evaluate other parameters.

References

1. Federal Emergency Management Agency and National Institute of Building Science. HAZUS (1999) *Earthquake Loss Estimation Methodology-Technical Manual.*
2. Schultz, M., Gouldby, B., Simm, J., and Wibowo, J. (2010) *Beyond the Factor of Safety: Developing Fragility Curves to Characterize System Reliability*. U.S. Army Engineer Research and Development Center, Environmental Laboratory and Geotechnical and Structures Laboratory. Oxfordshire, OX109BA, UK.
3. Singhal, A. and Kiremidjian, A. (1998) Bayesian Updating of Fragilities with Application to RC Frames. *Journal of Structural Engineering*, **124**(8), 922-929.
4. Rossetto, T. and Elnashai, A. (2003) Derivation of Vulnerability Functions for European-Type RC Structures Based on Observational Data. *Journal of Structural Engineering*, **25**(10), 1241-1263.
5. Ellinwood, R. (2008) structural reliability and performance-based. *Engineering Structures and Buildings*, **161**(4), 199-207.
6. Saez, E., Lopez-Caballero, F., and Modaressi-Farahmand-Razavi, A. (2011) Effect of the inelastic dynamic soil–structure interaction on the seismic vulnerability assessment. *Structural Safety*, **33,** 51–63.
7. Rizzitano, S., Cascone, E., and Biondi, G. (2014) Coupling of topographic and stratigraphic effects on seismic response of slopes through 2D linear and equivalent linear analyses. *Soil Dynamics and Earthquake Engineering*, **67**, 66–84.
8. Bouckovalas, G. and Papadimitriou, A. (2005) Numerical evaluation of slope topography effects on seismic ground motion. *Soil Dynamics and Earthquake Engineering*, **25**, 547-558.
9. Ashford, S.A, Sitar, N., Lysmer, J., Deng, N. (1997) Topographic effects on the seismic response of steep slopes. *Bulletin of the Seismological Society of America*, **87**, 701–709.
10. Tripe, R., Kontoe, S., and Wong, T.K.C. (2013) Slope topography effects on ground motion in the presence Of deep soil layers. *Soil Dynamics and Earthquake Engineering*, **50**, 72-84.
11. Assimaki, D. and Kausel, E. (2007) Modified Topographic Amplification Factors for a Single-Faced Slope due to Kinematic Soil-Structure Interaction. *Geotechnical and Geo environmental Engineering*, ASCE, **11**, 1414-1431.
12. Nasserasadi, K., Ghafory-Ashtiany, M., Eshghi, S., and Zolfaghari, M.R. (2009) Developing seismic fragility function of structures by stochastic approach. *Asian Journal of Civil Engineering (Building and Housing)*, **10**(2), 183-200.
13. Karavasilis, T., Bazeos, N., and Beskos, D. (2007) Behavior factor for performance-based seismic design of plane steel moment resisting frames. *Earthquake Engineering*, **11**, 531–59.
14. Eurocode 3 (1993) *Design of Steel Structures. Part 1-1: General Rules and Rules for Buildings*. European Committee for Standardization (Cen). Brussels.
15. Eurocode 8 (2005) *Design of Structures for Earthquake Resistance; Part 1: General Rules. Seismic Actions and Rules for Buildings*. European Committee for Standardization. Brussels.
16. Zerwer, A., Cascant, G., and Hutchinson, J. (2002) Parameter estimation in finite element simulations of rayleigh waves. *Journal of Geotechnical and Geoenvironmental Engineering*. **128**(3).
17. Ghanbari, A., Zarangzadeh, S., Rezaee, F., and

Sheikh-Zakariaee, S. (2011) Geotechnical Properties of central Part of Karaj Alluvium. *Scientific Quarterly Journal*, Geosciences, **25**(10), 1241-1263.

18. Bazazura, P. and Cornell, C. (1994) Seismic hazard analysis of nonlinear structures. *Structural Engineering*, **120**(11), 20-44.
19. Pacific Earthquake Engineering Research Center (PEER), Online Strong Motion Database, http://peer.berkeley.edu/smcat/ [2017, June 12].
20. Lin, L. (2012) Probabilistic seismic demand analysis using improved intensity measures. *15th World Conference on Earthquake Engineering*, Lisbon, Portugal.
21. Building and Housing Research Center (BHRC) (2014) *Iranian Code of Practice for Seismic Resistant Design of Buildings*. Standard No. 2800, 4th ed.